Spectroscopy of Coherent Dark Resonances in Samarium

J. V. Vladimirova,[a] B. A. Grishanin,[a] V. N. Zadkov,[a]
N. N. Kolachevsky,[b] A. V. Akimov,[b] N. A. Kiselev,[b] V. N. Sorokin[b] and S. I. Kanorski[b]

[a]Faculty of Physics and International Laser Center
M. V. Lomonosov Moscow State University, Moscow 119899, Russia
[b]P. N. Lebedev Physics Institute, Russian Academy of Sciences
Leninski ave. 53, Moscow 117924, Russia

ABSTRACT

A theoretical model of the coherent population trapping (CPT) in multilevel samarium atom and its comparison with experimental spectroscopic data are presented. Theoretical model describes a degenerated Λ-system in Sm atom formed of the transitions $4f^6 6s^2(^7F_0) \leftrightarrow 4f^6(^7F)6s6p(^3P^o)^9F_1^o \leftrightarrow 4f^6 6s^2(^7F_1)$ and includes also a fourth level $4f^6 6s^2(^7F_2)$, which complements the model making it an open system. An open character of the system reduces the contrast of the resonance curves in the CPT-spectra, but does not change the width of the CPT resonance. Numerical modeling of the CPT resonances in Sm atom was carried out for the case of applied longitudinal and transverse magnetic fields in 7- and 12-level models, as well.

Keywords: Coherent population trapping, dark resonance, samarium

1. INTRODUCTION

Coherent population trapping (CPT) phenomenon is currently widely used in different applications such as magnetometry, metrology, and others[1–5] and much attention in the literature has been paid so far to the alkali atoms.[6,7] In frequency standard applications (for cesium standard, see, for example Ref. [8]), rear-Earth atoms however have some advantages. By contrast with alkali atoms, their hyperfine structure energy levels are deeply shielded and, therefore, ground sublevels have much bigger energy splitting, on the order of 10–100 THz. Thus, direct coherent coupling of the dipole-allowed optical transitions in a Λ-system formed, for instance, of samarium atom hyperfine structure levels with rf transition between ground levels results in ultra-narrow, high-finess resonances in the *optical range*, which is an advantage for developing new frequency standards.

The basics of CPT phenomenon are well understood in the frame of three-level analytical model.[6] For the case of multilevel systems, however, the simple model has to be significantly complicated and analytical results in most cases became impossible. Enriched energetic structure of multilevel atoms results also in essential modification of the resonance dependencies on driving fields parameters. In this paper, we present a theoretical model for spectroscopy of coherent dark resonances in multilevel Sm atom and compare our theoretical calculations with experimental spectroscopic data for samarium.[10] While taking into account complete Zeeman structure of the involved levels requires a 12-level model, we show that a much simpler 4-level system gives already a reasonable agreement with the experimental observations.[10] This four-level model is formed of the degenerated Λ-system in Sm atom,

$$4f^6 6s^2(^7F_0) \leftrightarrow 4f^6(^7F)6s6p(^3P^o)^9F_1^o \leftrightarrow 4f^6 6s^2(^7F_1), \quad (1)$$

and the fourth level, $4f^6 6s^2(^7F_2)$, which complements the model making it an open system. An open character of the system reduces the contrast of the CPT-resonances, but does not change their widths. An extended 7- or 12-level model has also been used for simulation of the coherent dark resonances spectra in Sm in longitudinal and transverse magnetic fields, respectively.

Send correspondence to J.V.V.: vyulia@comsim1.phys.msu.su

ICONO 2001: Novel Trends in Nonlinear Laser Spectroscopy and Optical Diagnostics and Lasers in Chemistry, Biophysics, and Biomedicine, A. Yu. Chikishev, et al., Eds., SPIE Vol. 4749 (2002)

2. THREE-LEVEL MODEL

We will start with considering a three-level system in Λ-configuration, which is the simplest model for coherent dark resonances. Definitions of this Section will be used throughout the rest of the paper.

In a Λ-configuration, two bottom closely spaced energy levels $|1\rangle$ and $|2\rangle$, split at $\hbar\Delta$, are coupled with the upper lying energy level $|3\rangle$ by two driving laser fields (Fig. 1). If the transition $|1\rangle \leftrightarrow |2\rangle$ is forbidden in dipole approximation and two pumping fields $E_1 \exp(-i\omega_{L1}t - i\varphi_1)$, $E_2 \exp(-i\omega_{L2}t - i\varphi_2)$ are in the resonance with the driving transitions, one can register a sharp CPT-resonance, which reveals in absorption spectra as a sharp minimum when one of the driving fields, for instance with ω_{L1}, is scanned through the resonance point at the Raman detuning $\delta_R = \omega_{L1} - \omega_{L2} - \Delta = 0$.

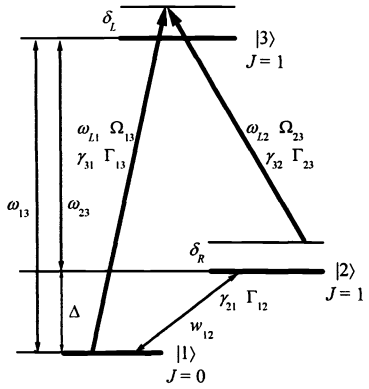

Figure 1. Energy diagram of a three-level atom in a Λ-configuration driven by two laser fields, ω_{L1} and ω_{L2}. Ω_{13} and Ω_{23} are the respective Rabi frequencies, γ_{31}, γ_{32}, and γ_{21} are the population decay rates, w_{12} is the pumping rate, Γ_{13}, Γ_{23}, and Γ_{12} are the pure dephasing rates, δ_L and δ_R are the laser and Raman detuning, respectively.

In theory, the CPT phenomenon could be understood in terms of two coherent linear combinations $|\pm\rangle$ of the ground states

$$|+\rangle = (\Omega_{R1}^*|1\rangle + \Omega_{R2}^*|2\rangle)/\Omega_{\text{eff}}, \quad |-\rangle = (\Omega_{R2}|1\rangle - \Omega_{R1}|2\rangle)/\Omega_{\text{eff}},$$

where $\Omega_{Rk} = -d_{3k}E_k/\hbar$ $(k = 1, 2)$ are the Rabi frequencies determined by the corresponding dipole moments d_{31}, d_{32}, and $d_{3k} = -e\langle 3|r|k\rangle$, and $\Omega_{\text{eff}} = \sqrt{|\Omega_{R1}|^2 + |\Omega_{R2}|^2}$.

In the rotating wave approximation (RWA), the matrix element of the dipole interaction operator for transition $|-\rangle \leftrightarrow |3\rangle$ is given by

$$\langle 3|V_{\text{dip}}|-\rangle = \frac{\hbar\Omega_{R1}\Omega_{R2}}{2\Omega_{\text{eff}}} e^{-i(\Omega_1+\omega_1)t - i\varphi_1} \left(1 - e^{i\delta_R t + i\Delta\varphi}\right), \tag{2}$$

where $\Delta\varphi = \varphi_2 - \varphi_1$ is the difference of the field phases $\varphi_{1,2}$. At the Raman resonance condition, this yields $\langle 3|\hat{V}_{\text{dip}}|-\rangle = 0$. As a result, such state absorbs and emits no photons. For the latter reason it is called the *coherent dark state.* The process of optical pumping in the presence of incoherent relaxation processes leads to the trapping of the entire population of the system in the dark state and reveals as the CPT resonance in absorption or transparency.

The coherent nature of the CPT determines, in accordance with Eq. (2), its dependence on the light phases $\varphi_{1,2}$. Therefore, phase fluctuations of the driving laser fields could decrease or even destroy the CPT-condition and stabilization of the relevant phases of the laser fields could be required. Other decoherence processes and Doppler broadening could be destructive factors for the CPT, as well.

3. EXPERIMENTAL SETUP

In experiment, two external-cavity diode lasers (ECDL) were tuned in resonance with the transition wavelengths in samarium: 672 nm and 686 nm. In Ref. 9 spectra of samarium transitions have been studied in detail using methods of sub-Doppler saturation spectroscopy. The relative isotopic shifts and hyperfine-structure splitting were determined with an accuracy of 1–2 MHz. It has also been shown that spectral lines of ^{154}Sm isotope (natural abundance of 22.75 %) are shifted with respect to the spectral lines of other isotopes by more than 1 GHz to the red, allowing us to lock reliably the lasers to the transitions of this isotope. Experimental setup we used for the dark resonances spectroscopy is shown in Fig. 2. The Sm vapor fills a 50 cm-long cell made of stainless steel with glass windows at the cell ends. The cell could be evacuated or filled with a buffer gas as required. A few grams of samarium were placed in the center of the cell. The 15-cm central part of the cell was heated by a coaxial dc-powered (~500 W) heating coil. The residual magnetic field inside the cell was a few fractions of an Oersted. The cell was heated to about 1000 K in order to obtain a noticeable absorption. The laser at 672 nm was locked to the corresponding transition in Sm . In Ref. 9 the frequency of this transition was measured to be 14863.7305 $\pm$ 0.0015 cm^{-1}. The laser at 686 nm was slowly scanned near the second transition of the Λ system, crossing the point where the Raman detuning is zero. Variation in the laser output frequency was monitored with a one-meter-long confocal interferometer, whose free spectral range was 75 $\pm$ 0.1 MHz. The single frequency operation of both lasers was controlled with a spectrum analyzer with a finess of 50 and a free spectral range of 8 GHz. To prevent a feedback, the interferometer was optically isolated from the lasers. The linearly polarized beams of both lasers were combined in a polarizing cube with an accuracy of 10^{-3} rad (Fig. 2). This beam illuminated the cell with samarium vapors. The beams transmitted through the cell were separated by a 2400 lines/mm holographic diffraction grating and entered a two-channel detection system.

The laser beam at 686 nm was modulated in front of the cell at the frequency 600 Hz using a liquid-crystal modulator, and then separated the modulated component from the detected signal of the other beam. In this way, we determined the change of the absorption of one of the beams introduced by the presence of the second beam.

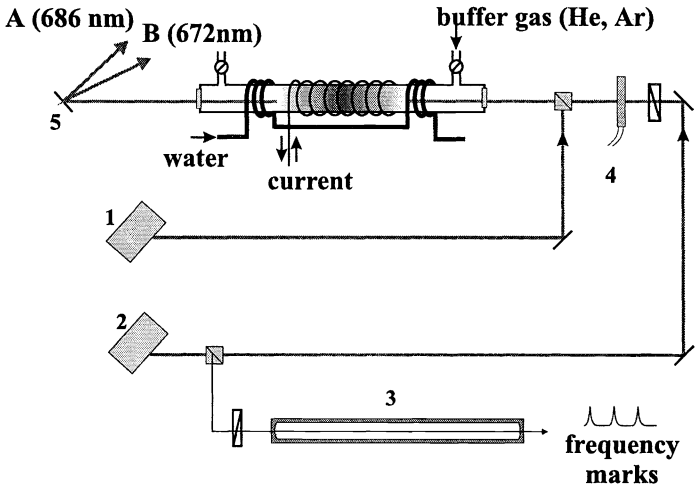

Figure 2. Experimental setup: 1—ECDL 672 nm, 2—ECDL 686 nm, 3—cavity (1 m), 4—modulator 600 Hz, 5—diffraction grating.

4. FOUR-LEVEL MODEL OF SAMARIUM ATOM

Energy levels diagram for Sm atom used in our calculations to model experimental dark resonances spectroscopy results is shown in Fig. 3a. It corresponds to the transitions (1). Tables 1 and 2 give oscillator strengths, energies, and g-factors of the lowest meta-stable levels with $J = 0, 1, 2$ and the upper $J = 1$ level, including the relative populations of the metastable levels at $T = 600°$ C (see Ref. 9).

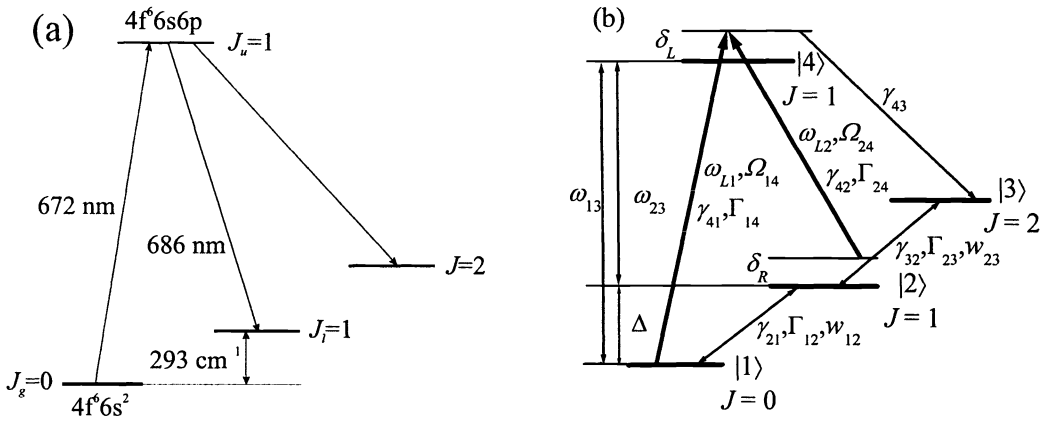

Figure 3. Energy levels diagram for samarium atom (a) and parameters used in our calculations (b). ω_{L1} and ω_{L2} are the laser frequencies, Ω_{14} are Ω_{24} are the corresponding Rabi frequencies, δ_L and δ_R are the detuning at the $|1\rangle \leftrightarrow |3\rangle$ transition and the Raman detuning, γ_{41}, γ_{42}, and γ_{43} are the radiation decay rates from the excited state to levels $|1\rangle$, $|2\rangle$, and $|3\rangle$; Γ_{14} and Γ_{24} are the pure dephasing rates for the transitions $|1\rangle \leftrightarrow |4\rangle$ and $|2\rangle \leftrightarrow |4\rangle$; γ_{21}, γ_{32} and w_{12}, w_{23} are the decay and pumping rates of the level $|1\rangle$ via the level $|2\rangle$ and $|2\rangle$ via the level $|3\rangle$; Γ_{12} and Γ_{23} are the pure dephasing rate of the $|1\rangle \leftrightarrow |2\rangle$ and $|2\rangle \leftrightarrow |3\rangle$ transition.

For comparison with experimental data we need to specify some experimental parameters to be plugged into our model. In the experiments on coherent dark resonances spectroscopy of samarium we used two semiconductor lasers tuned at 672 nm and 686 nm, respectively.[10] Both lasers operate in a single-frequency mode, at the average power of $W_{L1} = 2.5$ mW and $W_{L2} = 12$ mW, respectively. At the cell, input power densities are $W_{L1} = 0.1$ mW/mm^2 and $W_{L2} = 0.2$ mW/mm^2. Field strengths are given by formula $\sqrt{2W/c\varepsilon_0}$, where W is the laser power density, that yields $E_{L1} = 274$ V/m and $E_{L2} = 388$ V/m.

The magnetic field strength used in our experiments was about 20 Oe: 15 Oe for the longitudinal field and 19 Oe for the transverse one. For the longitudinal magnetic field, the corresponding Zeeman splitting $\Delta = egH/2mc$ is $\Delta' = 1.98 \times 10^8$ s^{-1} for the level 6s6p and $\Delta'' = 4.09 \times 10^8$ s^{-1} for the level 6s^2. For the transverse magnetic field, $\Delta' = 2.50 \times 10^8$ s^{-1} for the level 6s6p and $\Delta'' = 5.17 \times 10^8$ s^{-1} for the level 6s^2.

The dipole moment d, the Rabi frequencies Ω, and decay rates γ are calculated as:

$$|d_{JJ'}|^2 = (3\hbar e^2/2m)(2J+1)|f_{JJ'}|/\omega_{JJ'},$$

Table 1. Transition oscillator strengths for samarium.

Transition	Wavelength, nm	Oscillator strength, f
6s^2 ($J = 0$) → 6s6p ($J = 1$)	672.5875	8.5×10^{-3}
6s^2 ($J = 1$) → 6s6p ($J = 1$)	686.0927	9.5×10^{-3}

Table 2. Energy levels in samarium, which contribute to the absorption spectrum.

Even levels 4f^{6}6s^2(^{7}F)				Odd level 4f^6(^{7}F)6s6p(^{3}P°)^{9}F$^\circ_1$		
J	Energy, cm^{-1}	g	Relative population at $T = 600°$ C	J	Energy, cm^{-1}	g
0	0.00	—	1.0			
1	292.58	1.50	0.6	1	14863.85	3.10
2	811.92	1.50	0.24			

$$\Omega_{JJ'} = d_{JJ'}E/\hbar, \quad \gamma_{JJ'} = 4d_{JJ'}^2\omega^3/3\hbar c^3,$$

where m and e are the electron mass and charge, respectively, c is the speed of light, and $\omega_{JJ'}$ is the transition frequency. Table 3 summarizes these values for samarium. Non-zero values of parameters γ_{21}, γ_{32} are due to the time-of-flight broadening. The pumping rates w_{12}, w_{23} are related to the rates γ_{21}, γ_{32} via the temperature equilibrium condition.

Table 3. Parameters of the Λ-system for our model of samarium.

Rabi frequency, s^{-1}	Radiation decay rate, s^{-1}	Incoherent pumping rate, s^{-1}	Decay rate of the ground state, s^{-1}
$\Omega_{14} = 1.75 \times 10^7$	$\gamma_{41} = 1.25 \times 10^6$	$w_{12} = 2.4 \times 10^4$	$\gamma_{21} = 4.0 \times 10^4$
$\Omega_{24} = 2.65 \times 10^7$	$\gamma_{42} = 1.34 \times 10^6$	$w_{23} = 1.6 \times 10^4$	$\gamma_{32} = 4.0 \times 10^4$
—	$\gamma_{43} = 1.25 \times 10^6$	—	—

5. CALCULATION TECHNIQUE

Temporal dynamics of a multilevel system driven by laser fields can be written with the Liouville equation

$$\frac{d\hat{\rho}}{dt} = \mathcal{L}\hat{\rho}, \tag{3}$$

where $\mathcal{L}$ is the system Liouvillian, which takes into account both reversible and relaxation dynamics. For an N-level atom in the presence of laser fields it is written as a sum of contributions $\mathcal{L} = \mathcal{L}_r + \mathcal{L}_e + \mathcal{L}_\delta + \mathcal{L}_i$, where $\mathcal{L}_r$, $\mathcal{L}_e$, $\mathcal{L}_\delta$, and $\mathcal{L}_i$ are the contributions due to the radiation decay, pure dephasing, detuning of the laser fields, and laser–field interaction, respectively. As it is shown in Ref. [11], it is possible to combine the advantages of the symbolic and matrix representations with the possibilities of analytic computation and then effectively calculate the $N^2 \times N^2$-matrix representation for $\mathcal{L}$, L_r, L_e, L_δ, and L_i even for large N, making use of the following formula

$$L_{mn} = (\hat{e}_m, \mathcal{L}\hat{e}_n),$$

where $\hat{e}_n$ is a properly chosen operator basis of the matrix representation.[11] The spectrum calculation problem is significantly simplified for a stationary case, when it is only necessary to calculate the vector representation $\langle 0|$ of the stationary density matrix $\hat{\rho}_{st}$ as a solution of the null-space matrix problem $\langle 0|L = 0$. With this solution, it is possible to calculate any stationary average value of interest, i.e., absorption of the probe field.

For numerical calculations of the atomic populations and absorption/dispersion a specially designed Fortran-based program, which employs the shortly described above calculation technique, have been developed. Key advantage of this program (and algorithm) is that it requires only minimum number of active parameters that is significantly less than the total number N^4 of the matrix elements in the Liouville Eq. (3). Another advantage of the program is that it can be used (and has been tested) for any model of an atom with the number of energy levels $N \lesssim 20$. For larger dimensionality, additional efforts in testing the program are required.

6. COMPUTER SIMULATION RESULTS

The absorption coefficient in our four-level system modeling Sm atom is shown in Fig. 4b. For comparison, the absorption coefficient in the three-level model is shown in Fig. 4a, as well. Analysis of the dependencies of Fig. 4a,b shows that introducing of the fourth level $J = 2$ into the three-level model leaves the resonance width almost unchanged, whereas the full absorption of the four-level system is about an order of magnitude smaller than the absorption in the three-level model. This is due to the population trapping at the $J = 2$ level via the corresponding radiation decay channel.

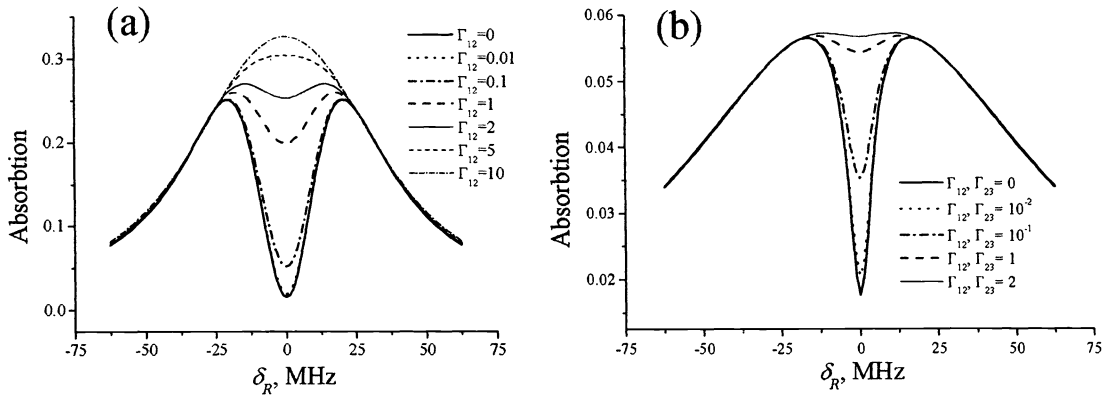

Figure 4. Absorption coefficient in the three-level (a) and four-level (b) models versus Raman detuning δ_R at $\delta_L = 0$ and different dephasing rates (s^{-1}). Corresponding models are shown in Figs. 1, 3.

6.1. Modification of the dark resonances in applied magnetic field

In the presence of a magnetic field, the considered above model of Sm atom transforms into a seven-level model due to the fact that levels with $J = 1$ split into three components each. As a result, splitting of the level $|3\rangle$ results in three allowed by the selection rules transitions to the level $|1\rangle$, the probability of each being 1/3 of the total transition probability $|3\rangle \leftrightarrow |1\rangle$. Similarly, splitting of the level $|2\rangle$ results in 6 allowed transitions to the levels $|2\rangle$ and $|3\rangle$ with the probability 1/6 of the total $|3\rangle \leftrightarrow |2\rangle$ transition probability.

For the following consideration we should distinguish between two configurations of the applied magnetic field—longitudinal and transverse configurations.

6.1.1. Longitudinal configuration of the applied magnetic field

Energy levels diagram for Sm atom, corresponding to the applied longitudinal magnetic field configuration, is shown in Fig. 5. For crossed linear polarizations of the driving system laser fields the selection rules allow six transitions because $E_1 \perp H$ ($\Delta m_1 = \pm 1$) and $E_2 \perp H$ ($\Delta m_2 = \pm 1$). Transitions $|1\rangle \leftrightarrow |5\rangle$ and $|3\rangle \leftrightarrow |5\rangle$, $|1\rangle \leftrightarrow |7\rangle$ and $|3\rangle \leftrightarrow |7\rangle$ form two three-level Λ-systems. Transitions $|2\rangle \leftrightarrow |6\rangle$ and $|4\rangle \leftrightarrow |6\rangle$ are also allowed by the selection rules, but they are not active in the excitation of the mentioned Λ-systems.

Depolarization due to the collisions could be an additional decay channel in a multilevel model, by contrast to the three-level model. A mechanism of this depolarization is the collision-induced transitions between the states with different values of the atom's moment onto a fixed direction. In the applied magnetic field, collisions induce transitions between the Zeeman sublevels with different values of magnetic moment for each multiplet. In our case, the CPT resonance occurs at the coherent superposition of the levels $|1\rangle$, $|3\rangle$ (Fig. 5). For momentum changing collisions, the coherence between levels $|1\rangle$ and $|3\rangle$ is destroyed because the population of the level $|3\rangle$ changes. The results of the absorption coefficient calculations for the complete 7-level model (Fig. 5) taking into account the magnetic sublevels depolarization, G_{magn}, are shown in Fig. 6. As it can be seen from Fig. 6, the depolarization process leads to the increase of the induced absorption and, additionally, in monotonous decrease of the CPT-resonance contrast. The depolarization does not change the width of the CPT-resonance.

Let us now find the conditions of the CPT-resonance for considered models. For both driving laser fields only transitions with $\Delta m = \pm 1$ are possible. Laser field with the frequency ω_{L1} is in resonance with the atoms velocity projections $v_x^{m=\pm 1}$ of which on the **k**-vector of the laser beam satisfy the following equation:

$$\omega_{L1} = (\omega_{13} \pm \Delta'')(1 + v_x^{m=\pm 1}/c). \tag{4}$$

The CPT condition is satisfied only if the atoms are in the resonance with the second laser frequency, ω_{L2}:

$$\omega_{L2} = (\omega_{23} \pm \Delta')(1 + v_x^{m=\pm 1}/c). \tag{5}$$

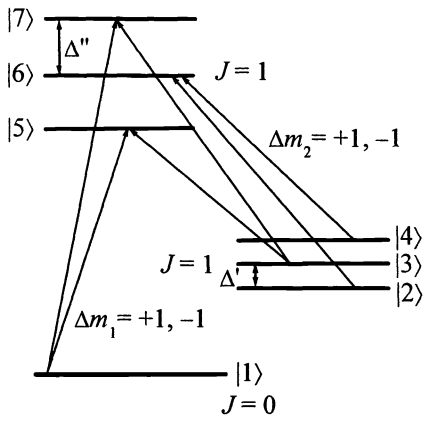

Figure 5. Energy levels diagram for Sm atom in the longitudinal magnetic field for the crossed linear polarization vectors of the driving laser fields. The selection rules for the laser fields with ω_{L1} and ω_{L2} are $\Delta m_1 = \pm 1$ and $\Delta m_2 = \pm 1$, respectively. Δ' and Δ'' are the Zeeman splittings of the lower and upper levels with $J \neq 0$, correspondingly.

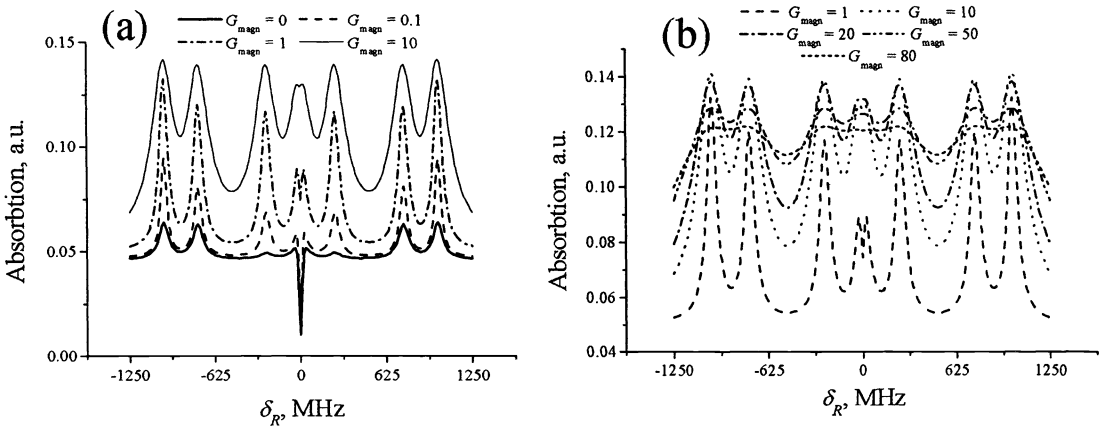

Figure 6. Absorption coefficient of the seven-level system (Fig. 5) versus Raman detuning δ_R at $\delta_L = 0$ and depolarization constant of the magnetic sublevels ranging from 0 to 10 (a) and from 1 to 80 (b).

It follows from Eqs. (4)–(5) that the CPT-resonance is achieved at the two frequencies of the probe laser, $\omega_{L2} = \omega_{23} \pm \omega_{12}(\Delta''/\omega_{13})$, which means that the CPT-resonance line is split at the frequency $2\Delta'(\omega_{12}/\omega_{13})$. Additional absorption lines at the frequencies $\pm 2\Delta''$, $\pm(\Delta' + \Delta'')$, and $\pm\Delta'$ correspond to the simultaneous excitation of the two transitions that do not form the Λ-system. For example, transition at the frequency $\omega_{23} + 2\Delta''$ corresponds to the resonance excitation of the transitions $|1\rangle \leftrightarrow |6\rangle$ and $|3\rangle \leftrightarrow |7\rangle$.

The comparison of calculated absorption spectrum in the 7-level model with the experimental spectrum of Sm atoms vapor is shown in Fig. 7. Shown spectra are the probe laser field (672 nm) absorption spectra, received by scanning the second driving laser field frequency. Fig. 7 show good correspondence between the experimental and theoretical spectra. Fitting of theoretical and experimental data shows the best results at $G_{\text{magn}} = 0$, which reveals a negligibly small interplay of the depolarization at the CPT in Sm atoms. Typical width of the experimentally observed CPT resonances is on the order of 5–6 MHz, which corresponds well with our theoretical calculations.

6.1.2. Transverse configuration of the applied magnetic field

Energy levels diagram for Sm atom, corresponding to the applied transverse magnetic field configuration, is shown in Fig. 8.

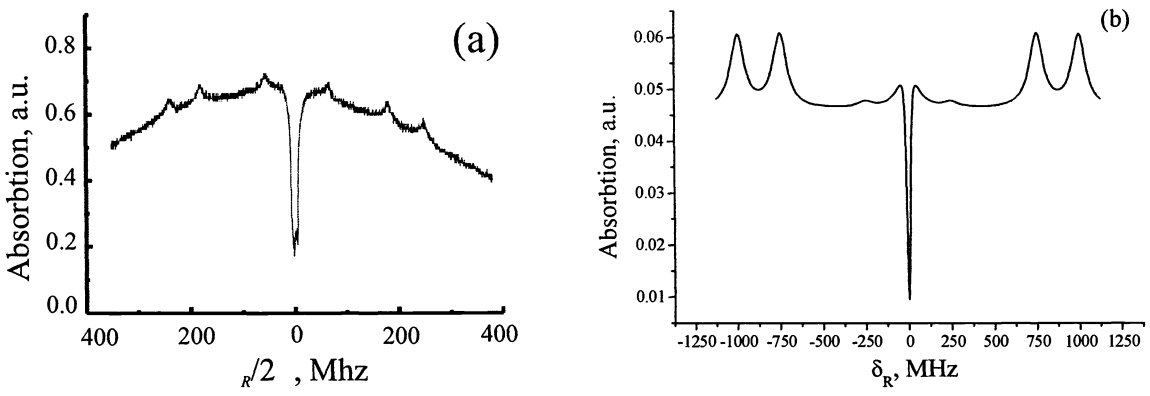

Figure 7. a) Experimental absorption spectrum of Sm vapor versus Raman detuning δ_R in the presence of a longitudinal magnetic filed. The magnetic field strength is 19 Oe and the buffer gas (Ar) pressure—0.2 Torr. b) Calculated absorption spectrum of Sm atom in the seven-level model (Fig. 5) versus Raman detuning δ_R at $\delta_L = 0$ and the magnetic sublevels depolarization constant $G_{\text{magn}} = 0$.

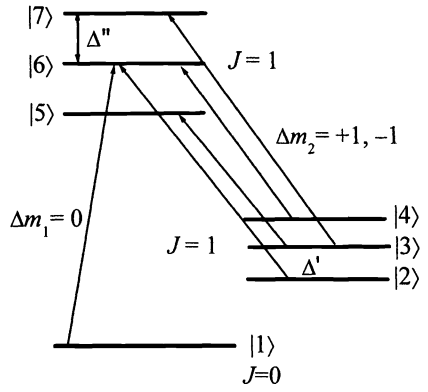

Figure 8. Energy levels diagram for Sm atom in the transverse magnetic field for the crossed linear polarization vectors of the driving laser fields. The selection rules for the laser fields with ω_{L1} and ω_{L2} are $\Delta m_1 = 0$ and $\Delta m_2 = \pm 1$, respectively. Δ' and Δ'' are the Zeeman splittings of the lower and upper levels with $J \neq 0$, correspondingly.

In a transverse magnetic field $H_\perp$, a linear polarization of the laser field with ω_{L1} ($\vec{H}_\perp$ lies in the polarization plane) may induce only the transitions with $\Delta m = 0$, which are π-components. At the same time, the laser field with ω_{L2} with the polarization plane orthogonal to $H_\perp$ induces the transitions with $\Delta m = \pm 1$, which are σ-components. In this case, two Λ-systems, corresponding to the transitions $|1\rangle \leftrightarrow |6\rangle$, $|2\rangle \leftrightarrow |6\rangle$ and $|1\rangle \leftrightarrow |6\rangle$, $|4\rangle \leftrightarrow |6\rangle$, are excited, whereas the transitions $|3\rangle \leftrightarrow |5\rangle$ and $|3\rangle \leftrightarrow |7\rangle$ are not active.

The influence of the depolarization of the magnetic sublevels reveals in the absorption coefficient and the parameters of the CPT-resonance similarly to the case of longitudinal magnetic field (Sec. 6.1.1). The calculation results for different depolarization constant values are shown in Fig. 9. The maximum of the resonance contrast is achieved at $G_{\text{magn}} = 0$. It can also be easily seen that increasing G_{magn} reduces the CPT-resonance contrast, whereas its width remains almost the same. Similarly to the case of longitudinal magnetic field, we can calculate positions of the CPT lines in the Doppler broaden spectrum for a transverse magnetic field. This spectrum yields also a splitted CPT-resonance line and the splitting value coincides with the Zeeman splitting of the sublevels $|2\rangle$ and $|4\rangle$ of the lower level $J = 0$: $\Delta\omega = 2\Delta'$. The splitting ratio of the CPT-resonances for longitudinal and transverse magnetic

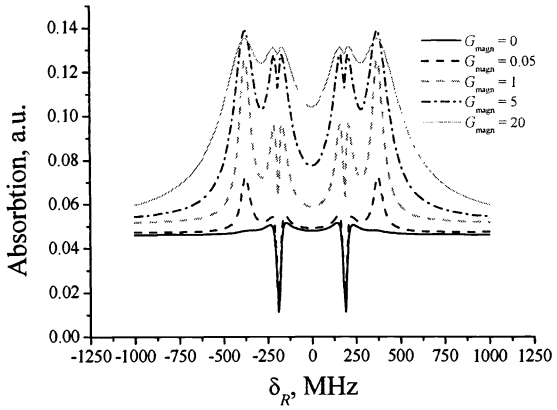

Figure 9. Absorption coefficient of the seven-level system (Fig. 8) versus Raman detuning δ_R at $\delta_L = 0$ and depolarization constant of the magnetic sublevels ranging from 0 to 80.

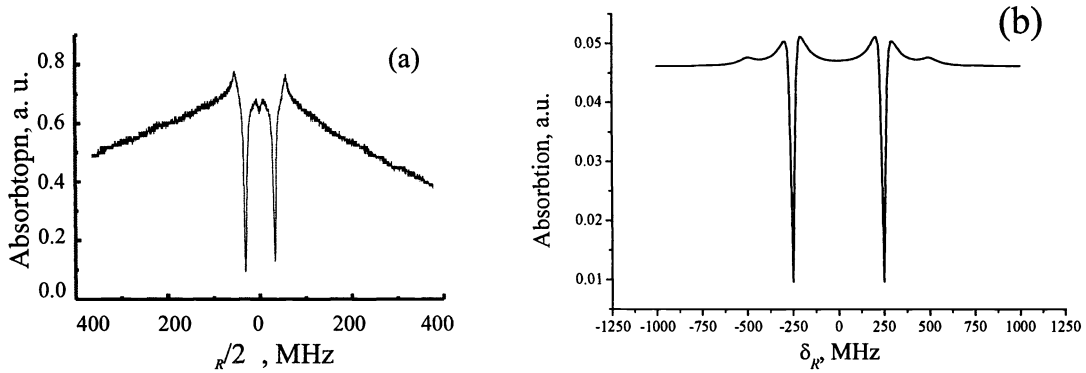

Figure 10. a) Experimental absorption spectrum of Sm vapor versus Raman detuning δ_R in the presence of a transverse magnetic filed. The magnetic field strength is 19 Oe and the buffer gas (Ar) pressure—0.2 Torr. b) Calculated absorption spectrum of Sm atom in the seven-level model (Fig. 5) versus Raman detuning δ_R at $\delta_L = 0$ and the magnetic sublevels depolarization constant $G_{\text{magn}} = 0$.

fields reads

$$\frac{\Delta\omega_\perp}{\Delta\omega_\parallel} = \left(\frac{\Delta'_\perp}{\Delta'_\parallel}\right)\left(\frac{\omega_{12}}{\omega_{13}}\right) = \frac{H_\perp}{H_\parallel}.$$

7. CONCLUSIONS

In conclusion, we present a theoretical model for the coherent dark resonances spectroscopy for a multilevel atom, which takes into account all the coherences and decay rates in the system, as well as possible pumping rates and driving system laser fields. Such a model allows to fit any real multilevel atom. The model was adjusted for the samarium atom and the comparison with our experimental spectroscopic data is presented. It is shown that multilevel energy structure of Sm atom without external magnetic field can be well fit in a simple four-level model, whereas 7- and 12-level models work well for the cases of applied longitudinal and transverse magnetic fields, respectively.

ACKNOWLEDGMENTS

Authors from M. V. Lomonosov Moscow State University acknowledge partial support from the RFBR grant no. 01–02–16311, the State science-technical programs of the Russian Federation "Fundamental Metrology" and "Nano-

technology", and INTAS grant no. 00–479, and authors from P. N. Lebedev Physics Institute acknowledge partial support from the RFBR grants no. 01–02–174–42, 01–02–174–39, and 00–15–96–586 and Volkswagen-Stiftung grant I/73647.

REFERENCES

1. G. Alzetta, A. Gozzini, L. Moi, G. Orriols, Nuovo Cimento. B. **36**, 5 (1976).
2. H. R. Gray, R. M. Whitly, and C. R. Stroud (Jr), Opt. Lett. **3**, 218 (1978).
3. G. Alzetta, L. Moi, G. Orriols, Nuovo Cimento. B. **52**, 209 (1979); Opt. Commun. **42**, 335 (1982).
4. A. Aspect, E. Arimondo, R. Kaiser, N. Vansteenkiste, C. Cohen-Tannoudji, Phys. Rev. Lett. **61**, 826 (1996).
5. A. Kasapi, Phys. Rev. Lett. **77**, 3908 (1997).
6. E. Arimondo, "Coherent population trapping in laser spectroscopy", In: *Progress in Optics*, **35**, 257 (1996), E. Wolf, Ed. (Elsevier, Amsterdam).
7. R. Wynands, A. Nagel, Appl. Phys. B **68**, 1 (1999).
8. R. Holtzwarth, Th. Udem, and T. W. Haensh, Phys. Rev. Lett. **85**, 2264 (2000).
9. N.N. Kolachevskii, A.V. Akimov, N.A. Kiselev, A.A. Papchenko, V.N. Sorokin, S.I. Kanorski, Optics and Spectroscopy, **90(2)**, 164 (2001).
10. N.N. Kolachevski, A.V. Akimov, N.A. Kiselev, A.A. Papchenko, V.N. Sorokin, S.I. Kanorski, Quantum Electronics, **31(1)**, 61 (2001).
11. B. A. Grishanin, *Quantum Stochastic Processes*, located at http://comsim1.phys.msu.su/index.html (in Russian).